Axial-flux vs. radial-flux permanent-magnet synchronous generators for micro-wind turbine application

Adrian Augustin POP, Florin JURCA, Claudiu OPREA, Mihai CHIRCA, Stefan BREBAN, Mircea M. RADULESCU
TECHNICAL UNIVERSITY OF CLUJ-NAPOCA
22 Memorandumului street, 400114
Cluj-Napoca, Romania
Tel.: +40264 401 829.
E-Mails: Augustin.Pop@emd.utcluj.ro, Florin.Jurca@emd.utcluj.ro, Claudiu.Oprea@emd.utcluj.ro, Mihai.Chirca@mae.utcluj.ro, Stefan.Breban@emd.utcluj.ro, Mircea.Radulescu@emd.utcluj.ro
URL: http://www.utcluj.ro/

Keywords

«Permanent-magnet synchronous generator», «Direct drive», «Wind energy conversion systems», «Field analysis», «Design».

Abstract

This paper presents a comparative study between the axial-flux and radial-flux permanent-magnet synchronous generators for a 3 kW wind turbine application. This study emphasizes the most cost-effective solution to be implemented by the industrial partner. There are three constructive types of electric generators considered in this work. All are based on permanent-magnet synchronous generators (PMSGs), but one has an axial-flux topology, the other one is a radial-flux outer-rotor machine and the third one is a radial-flux inner-rotor machine. Finite-element field analysis was made for the three PMSGs in order to compare their efficiency and active materials estimated cost. The results show that the axial-flux PMSG is the best solution for micro-wind turbine application.

Introduction

Two major reasons are advocating for cost-effective micro-wind turbine power systems: the need to give a feasible alternative solution to classical and pollutant energy production and the need to make it affordable for the middle-class citizens, especially in Eastern-Europe where the GDP per capita is lower than in Western-Europe. This paper presents a part of the work endeavored to be made within a research project in partnership between the Technical University of Cluj-Napoca, Romania and an industrial small company. The solutions investigated are starting from a few premises: the micro-wind power system should be implemented mainly in urban areas, thus it should be very efficient in converting energy at low wind speeds; the electric generator is directly driven by the turbine and the associated electronic power converters should be controlled in a maximum-power-point-tracking strategy for connection to power grid, and should satisfy the voltage constraints for connection to isolated loads.

The three constructive types of wind-turbine generator considered in this work are permanent-magnet synchronous generators (PMSGs), but one has an axial-flux (AF-PMSG) topology, the other one is of radial-flux outer-rotor (RFOR-PMSG) type, while the third one is of radial-flux inner-rotor (RFIR-PMSG) type. In the following sections, each of the three PMSG topologies are investigated using finite-element field analysis to comparatively show their relative merits and demerits.

Axial-flux permanent-magnet synchronous generator (AF-PMSG)

Axial-flux (AF) PMSGs have a number of distinct advantages over their radial-flux counterparts, i.e. they can be designed to have (i) higher power-to-weight ratio, resulting in less core material,

(ii) planar and easily adjustable air-gaps, (iii) reduced noise and vibration levels. Moreover, the direction of the airgap flux path can be varied, so that additional topologies can be derived [1, 2].
The comparison of different AF-PMSGs is a difficult task. Many researchers try to force comparisons through subjective constraints. The outcome is often that the constraints themselves favor one configuration over the other, leading to inconclusive results and arbitrary selection.
There are possible many variations in the AF-PMSG basic design [3], including single-sided [4], double-sided [5], toroidal [6], and multi-disc designs. The AF-PMSG topology considered in this paper is a three-phase double-rotor one-stator topology with 8 pole-pairs, 3 kW rated power and 200 [rpm] rated speed. The magnets are of high-energy NdFeB-type, and are glued on both sides of the two solid-iron disc-rotors. The stator is made of non-magnetic material.
Slotted stators in the AF-PMSG machine increase notably the amplitude of the airgap flux density due to shorter airgap. This reduces the required amount of rotor-PMs, thus leading to savings in the AF-PMSG cost. Moreover, copper losses in slotted-stator AF-PMSG are lower than those of its slotless-stator counterpart. On the other hand, the use of slotted-stator armature winding results in significant cogging torque and content of harmonics in the back-emf waveform. Both problems may be tackled efficiently from the design point of view.
In [7] and [8], the authors reason the application of slotted-stator concentrated winding in AF-PMSGs. When concentrated windings are used, prefabricated coils can simply be inserted in the stator structure, and the winding process becomes cheaper. Furthermore, the space occupied by the end-windings and thus the corresponding Joule losses are minimized. However, due to the disposition of concentrated-winding coils there are space-harmonic components in the generated armature-reaction m.m.f.

Analytical preliminary design of the small-scale AF-PMSG

From the general sizing equation applied to the small AF-PMSG under study, the outer surface diameter D_o can be obtained as

$$D_0 = \left[\frac{8}{\pi^2} \frac{p}{f} \frac{P_{out}}{k_i k_p \eta (1+\lambda)(1-\lambda^2)(B_g)} \right]^{1/3} . \tag{1}$$

The total outer diameter of the considered AF-PMSG is given by

$$D_{tot} = D_0 + 2W_{Cu} . \tag{2}$$

The total axial length of the AF-PMSG can be expressed as

$$L_{tot} = L_r + 2L_S + 2g , \tag{3}$$

where the rotor axial length sums the rotor-core and rotor-PM contributions, i.e.

$$L_r = L_{r,core} + 2L_{PM} = B \frac{B_u}{B_{r,core}} \cdot \frac{\pi}{8} \frac{(1+\lambda)D_0}{p} + \frac{\mu_{r,PM} B_g}{B_{rem} - \frac{k_f}{k_d} B_g} k_c g \tag{4}$$

with $B_{r,core}$ defining the flux density in the rotor-disk core; B_u, the attainable flux density on the surface of the rotor-PM; $\mu_{r,PM}$ and B_{rem}, the relative permeability and the remanent flux density of the rotor-PM material, respectively; k_d and k_f, the leakage-flux factor and the peak-value-corrected radial-airgap-flux-density factor of the AF-PMSG, respectively; k_e , the back-emf factor, i.e. the armature-winding distribution factor; N_{ph} , the number of turns in series per armature-winding phase; f, the mains electrical frequency; p, the number of machine pole-pairs; D_i , D_o , the diameters of the inner and outer surfaces of the AF-PMSG, respectively; $\lambda=D_i / D_o$, the inner-to-outer diameter ratio; $\hat{B}_g$, the peak value of the magnetic flux density in the airgap (magnetic loading); g, the airgap axial length; k_C, the Carter factor, which takes into account the fact that large airgap length in front of the stator-slot and a small one in front of the stator-tooth makes the airgap flux density position-dependent; k_C can be expressed as [1, 6]

ISBN: 978-90-75815-17-7 and 978-1-4799-0114-2

$$k_c = \frac{t}{t - \gamma g}, \qquad \gamma = \frac{4}{\pi}\left[\frac{W_{so}}{2g}\tan^{-1}\left(\frac{W_{so}}{2g}\right) - \ln\sqrt{1 + \left(\frac{W_{so}}{2g}\right)^2}\right] \tag{5}$$

γ and W_{so} being the average slot-pitch and the slot-opening, respectively.

The stator axial length is

$$L_S = L_{s,core}, \tag{6}$$

where $$L_{s,core} = \frac{B_g}{B_{s,core}} \cdot \frac{\pi}{4} \frac{\alpha_p (1+\lambda) D_0}{p} \tag{7}$$

with $B_{s,core}$, denoting the flux density in the stator core; α_p, the ratio of the average-to-peak airgap flux density; J_{slot}, the stator-slot current density; k_{Cu}, the copper-fill factor.
The design specifications and chosen parameters have been considered in determining the main dimensions of rotor and stator components of the small-scale three-phase AF-PMSG, which are listed in Table 1.

3-D finite-element field analysis of the small-scale AF-PMSG

Finite-element (FE) simulations are performed in JMAG Designer 12.0 [9], an electromagnetic field analysis software package that supports the design and development of electric machines, actuators, circuit components etc. Two types of FE simulations are carried out: in no-load (open-circuit) and resistive-load conditions [10].
In order to analyze the performances of the considered small-scale three-phase AF-PMSG, its 3D-model is first constructed, as shown in Fig.1.

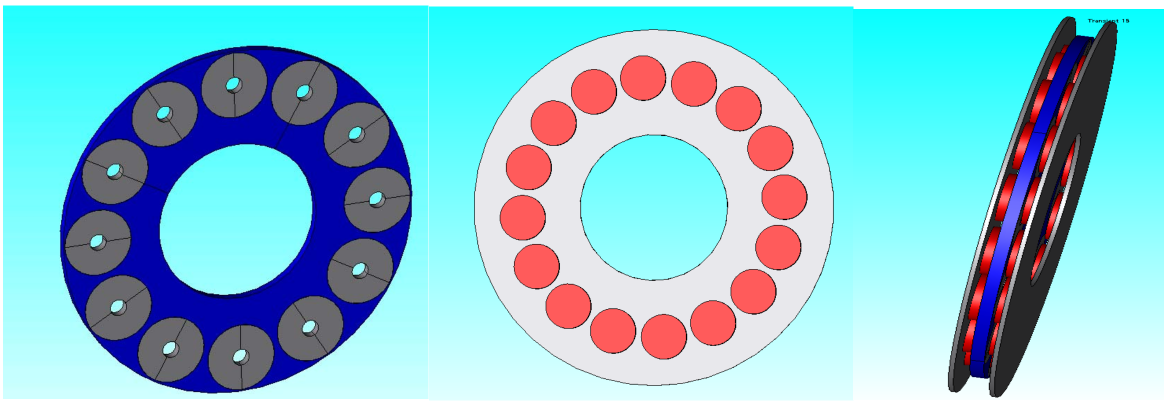

Fig. 1: 3D-model of the three-phase small-scale AF-PMSG topology [9].

The AF-PMSG has a double-rotor-one-stator topology. Rotor-PMs are of Nd-Fe-B 35SH type with axial magnetization. The PM-excitation flux of each rotor-pole travels through the sandwiched-stator and the two axial air gaps to the opposite rotor.
The three-phase stator-winding comprises 2000 [turns/ phase] of 12 [Ω] electrical resistance.
FE simulations are carried out for the three-phase small-scale AF-PMSG running at 200 [rpm] rated speed, under open-circuit and three-phase resistive load of 100 [Ω/phase] conditions, respectively. The simulation results are captured on JMAG Designer and presented in Fig.2. It can be seen that the phase back-emf waveforms have amplitudes of approximately 400 [V/phase] at open-circuit (no-load) and 300 [V/phase] at resistive-load conditions
The magnetic flux density distribution for the small-scale AF-PMSG under study is presented in Fig. 3, showing that there are not saturated zones for this design under no-load and resistive-load conditions.

ISBN: 978-90-75815-17-7 and 978-1-4799-0114-2

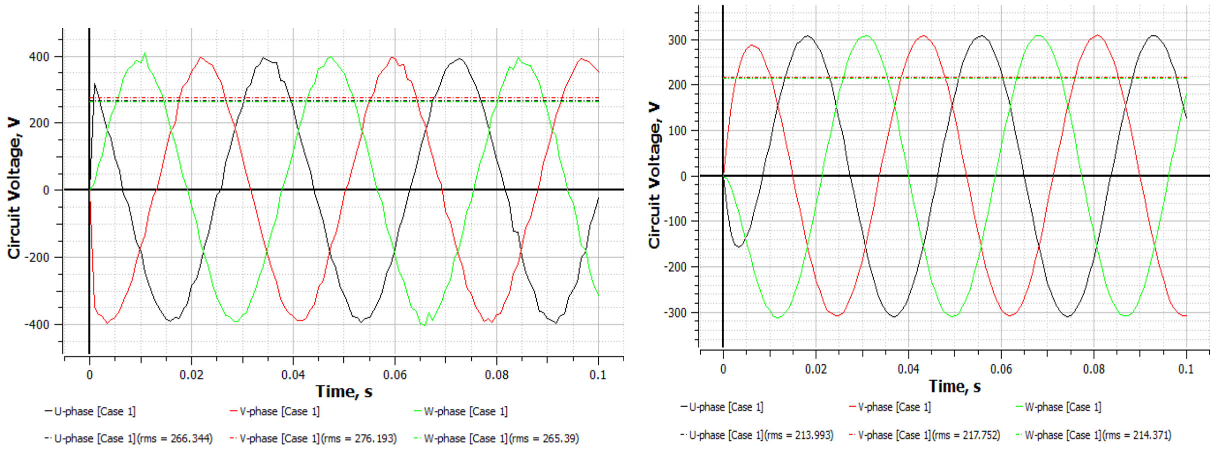

(a) (b)

Fig. 2: Back-emf waveforms of the three-phase small-scale AF-PMSG under (a) no-load (open-circuit) and (b) balanced resistive-load conditions, at rated rotor speed.

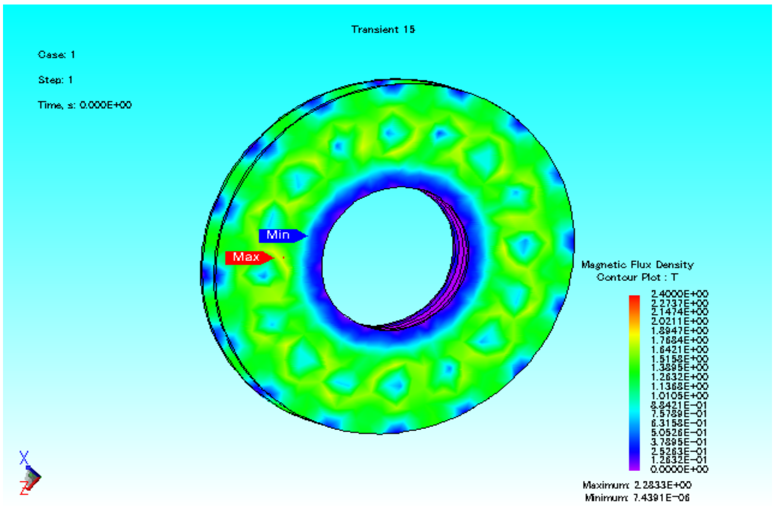

Fig. 3: Magnetic flux-density distribution for the three-phase small-scale PMSG.

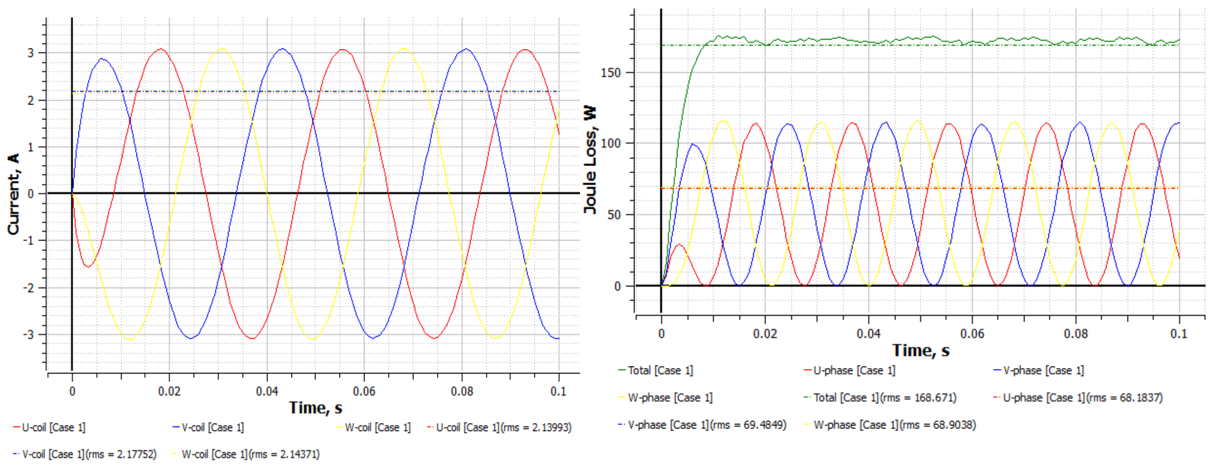

(a) (b)

Fig. 4: Phase-current (a) and Joule-loss (b) waveforms of the three-phase small-scale AF-PMSG with balanced resistive load.

 ISBN: 978-90-75815-17-7 and 978-1-4799-0114-2

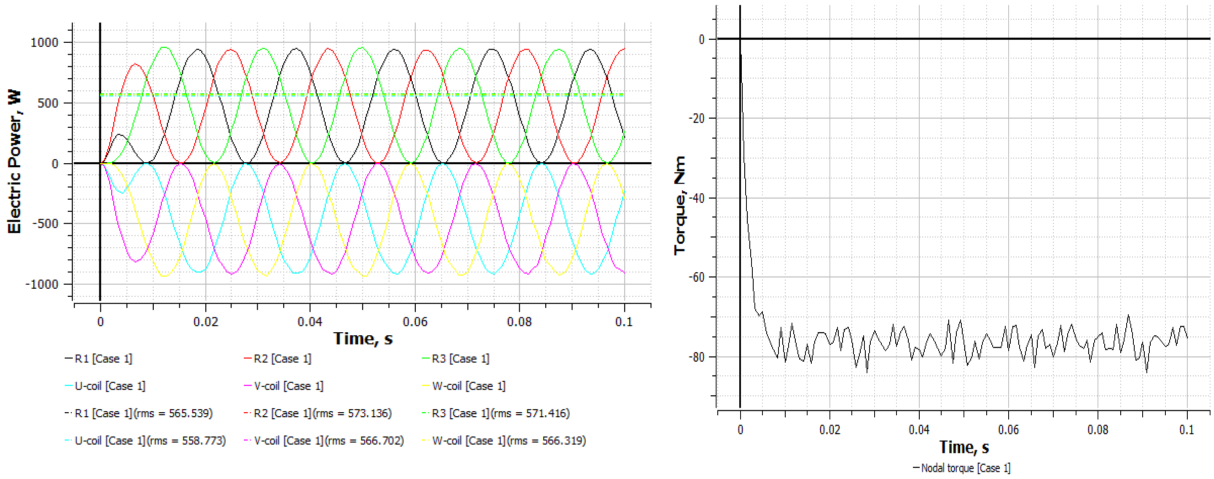

(a) (b)

Fig. 5: Electric power / phase and electromagnetic torque of the three-phase small-scale AF-PMSG at balanced resistive-load conditions.

For the three-phase small-scale AF-PMSG under preset resistive-load conditions, the FE-simulated phase current and Joule loss waveforms are shown in Fig. 4.

The developed electric power / phase and electromagnetic torque of the three-phase small-scale AF-PMSG with balanced resistive load are presented in Fig. 5.

Radial-flux outer-rotor permanent-magnet synchronous generator (RFOR-PMSG)

The radial-flux outer-rotor permanent-magnet synchronous generator (RFOR-PMSG) considered here has 15 pole-pairs. The advantage of RFOR-PMSG compared to inner-rotor PMSG is that the magnets are more easily attached to the rotor surface (Fig. 6).

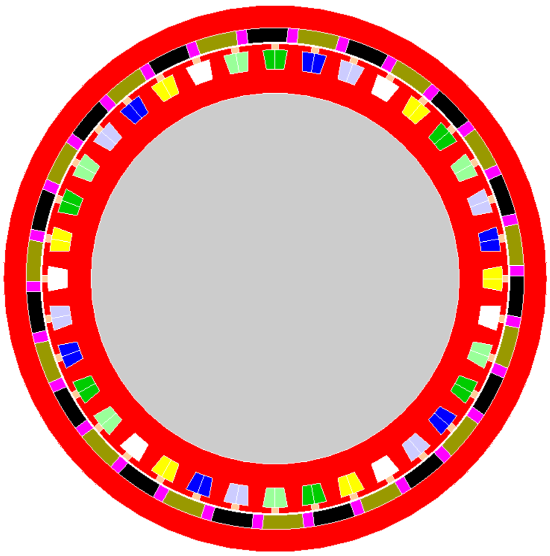

Fig. 6: Three-phase small-scale RFOR-PMSG topology.

As well known, the output power of an electric machine, when the leakage reactance is neglected, is proportional to the number of phases of the machine, n_{ph}, the phase current, $i(t)$, the induced emf, $e(t)$:

$$P_{out} = \eta \cdot \frac{n_{ph}}{T} \cdot \int_0^T e(t) \cdot i(t) dt = \eta \cdot n_{ph} \cdot k_p \cdot E_{max} \cdot I_{max} \,, \qquad (8)$$

 ISBN: 978-90-75815-17-7 and 978-1-4799-0114-2

where T is the period of an emf cycle; E_{max} and I_{max} represent the peak values of the emf and phase current, respectively; k_p is the power coefficient, and η is the estimated efficiency. The peak value of the emf is expressed by introducing the emf coefficient, k_E:

$$E_{\max} = k_e \cdot N_t \cdot B_{gap} \cdot D_{gap} \cdot L_m \cdot \frac{f_s}{p}, \tag{9}$$

where N_t is the number of turns per phase, B_{gap} and D_{gap} are the air-gap flux density and diameter, L_m is the length of the machine, f_s is the supplying frequency and p is the number of pole-pairs [11].
By introducing geometric coefficient, $k_L=L_m/D_{gap}$, and current coefficient (related to its waveform) $k_i=I_{max}/I_{rms}$, and defining the phase load ampere-turns,

$$A_t = \frac{2}{\pi} \cdot N_t \cdot \frac{I_{rms}}{D_{gap}}, \tag{10}$$

it is possible to define the airgap diameter of the machine:

$$D_{gap} = \sqrt[3]{\frac{2 \cdot p \cdot P_{out}}{\pi \cdot n_{ph} \cdot A_t \cdot k_e \cdot k_i \cdot k_p \cdot k_L \cdot \eta \cdot B_{gap} \cdot f_s}}. \tag{11}$$

Based on the type of the current waveform, it is possible to define the current and power coefficients for sinusoidal waveform [10], $k_i = \sqrt{2}, k_p = 0.5$.All the other geometric parameters will be computed based on this airgap diameter.
The RF-PMSG designer has to choose only the PMs shape and stator slots. As materials for active parts of the machine, Nd-Fe-B PMs with 1.2 [T] remanent flux density and M530-50A steel laminations are used.
FE simulations for the considered three-phase small-scale RFOR-PMSG are carried out using Flux2D software. The magnetic flux-density distribution in the cross-section of the machine is presented in Fig. 7.

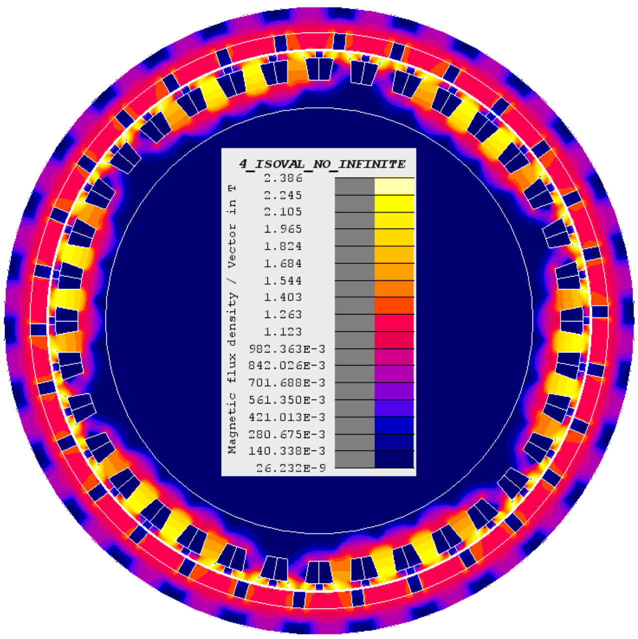

Fig.7: Magnetic flux-density distribution in the cross-section of the three-phase small-scale RFOR-PMSG.

For the three-phase small-scale RFOR-PMSG under no-load (open-circuit) and balanced resistive-load conditions, the FE-simulated back-emf waveforms are shown in Figs. 8 and 9, respectively, at rated rotor speed.

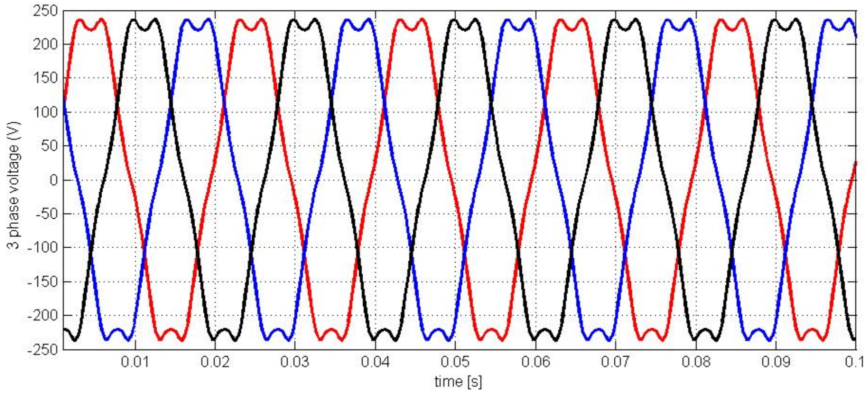

Fig. 8: Phase back-emf waveforms of the three-phase small-scale RFOR-PMSG under (no-load) open-circuit conditions, at rated rotor speed.

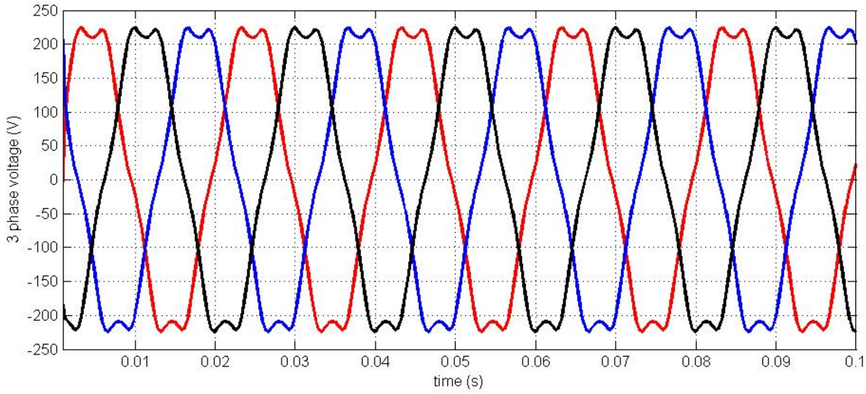

Fig. 9: Phase back-emf waveforms of the three-phase small-scale RFOR-PMSG with balanced resistive load, at rated rotor speed.

Radial-flux inner-rotor permanent-magnet synchronous generator (RFIR-PMSG)

The third three-phase small-scale PMSG topology considered here is a radial-flux inner-rotor (RFIR) one. For its preliminary design, the main geometric dimensions are obtained using the previously-sized RFOR-PMSG topology and the commercially-available electric-machine-design software SPEED, developed at the University of Glasgow, UK. The structure was dimensioned using version 9.1.2.29 of the software [12].
The chosen RFIR-PMSG structure has spoke-shaped, circumferentially-magnetized PMs, buried in the rotor (Fig.10). Due to the rotor-PM placement and magnetization, flux concentration in rotor poles toward the airgap results, and the same volume of PM material can be used for smaller airgap length. The number of stator slots / rotor poles and the three-phase winding configuration are the same as for the prior RFOR-PMSG.
By using SPEED software, extensive simulations have been performed and various geometric dimensions have been modified, in order to obtain optimal electric power, generated voltage and efficiency. The final design model has been exported in JMAG-Studio for checking its validity against FE simulations.
In Fig. 11, FE-simulations for magnetic flux-density distribution in the cross-section of the designed three-phase small-scale RFIR-PMSG, at no-load (open-circuit) and resistive load conditions are presented.

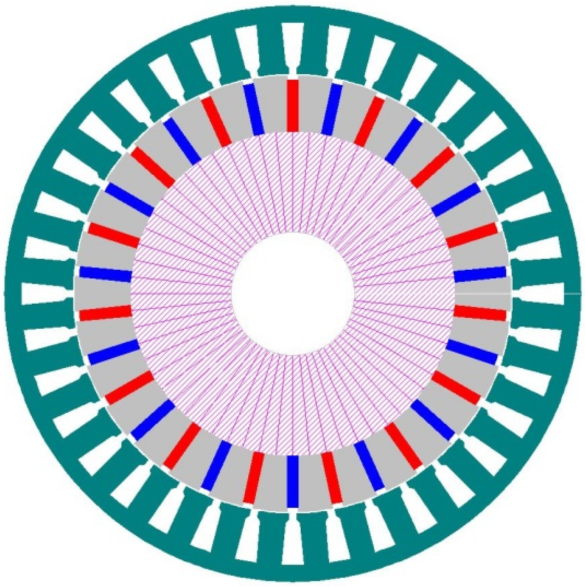

Fig. 10. Three-phase small-scale RFIR-PMSG topology
with spoke-shaped, circumferentially-magnetized PMs, buried in the rotor.

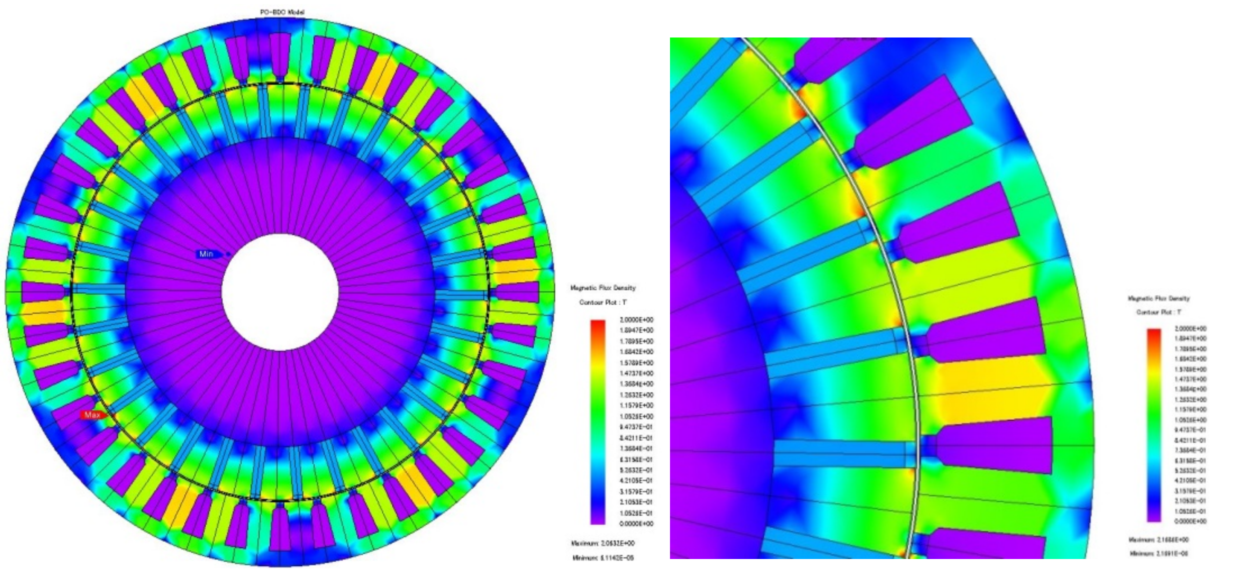

a) b)

Fig. 11: Magnetic flux-density distribution in the cross-section of the three-phase small-scale RFIR-PMSG, at no-load (a) and resistive-load (b) conditions.

For 120° rotation of the three-phase small-scale RFIR-PMSG under no-load (open-circuit) and balanced resistive-load conditions, the FE-simulated back-emf waveforms are shown in Fig. 12.

The generated phase currents and developed electromagnetic torque of the RFIR-PMSG with balanced resistive load are presented in Fig. 13.

 ISBN: 978-90-75815-17-7 and 978-1-4799-0114-2

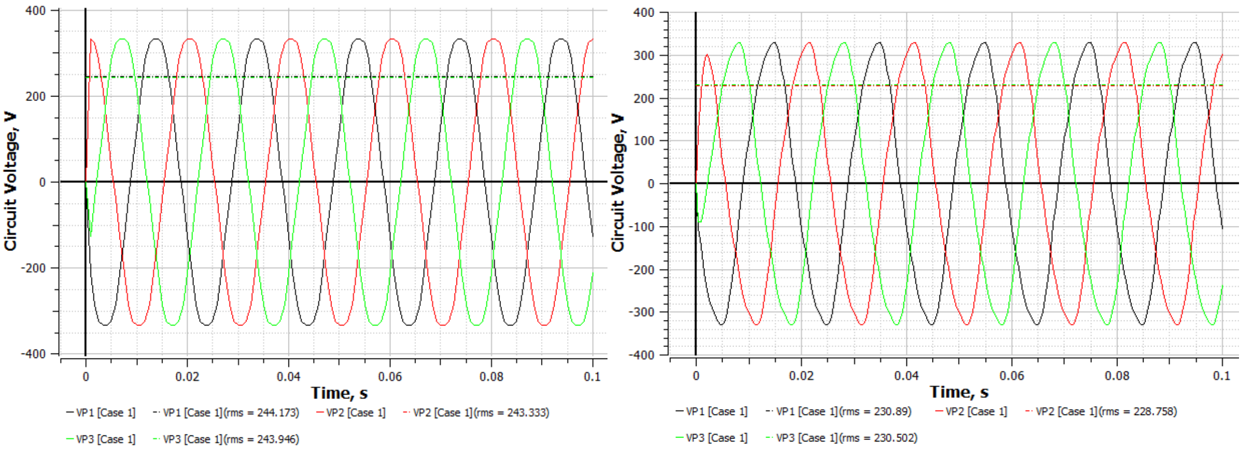

a) b)

Fig. 12: Back-emf waveforms of the three-phase small-scale RFIR-PMSG under (a) no-load (open-circuit) and (b) balanced resistive-load conditions.

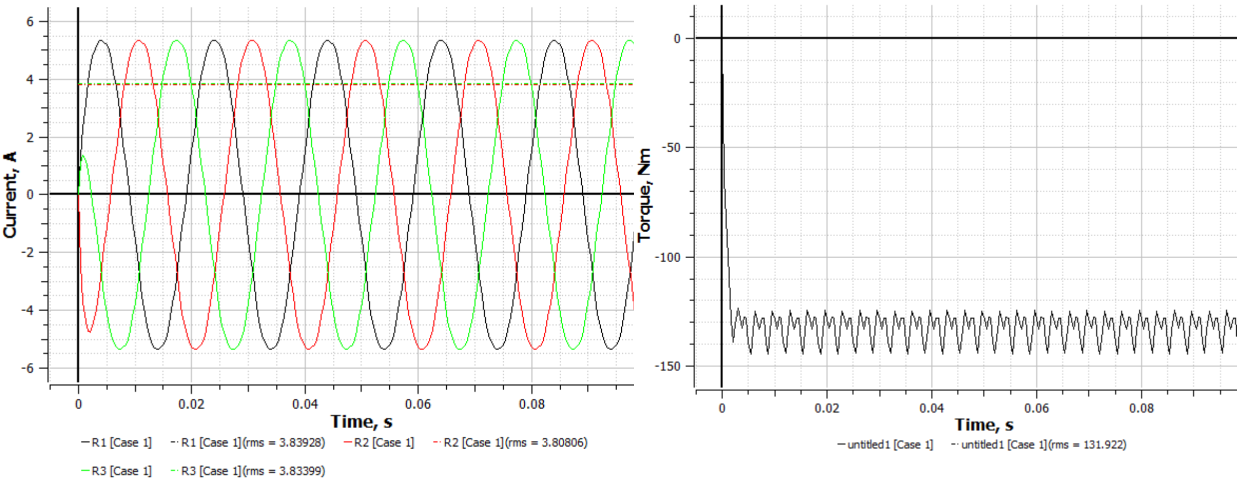

a) b)

Fig. 13: Generated phase currents and developed electromagnetic torque of the three-phase small-scale RFIR-PMSG at balanced resistive-load conditions.

Comparative results and discussion

The comparative main design results for the three small-scale PMSGs under study for micro-wind turbine application are summarized in Table I. The estimated costs of active materials, i.e. copper, PMs and iron (without considering the rotor shaft) are calculated. The reference prices for them are: 50 [Euro/kg] for PMs, 7.5 [Euro/kg] for copper and 3 [Euro/kg] for stator and / or rotor iron. These prices only refer to the raw materials, disregarding the manufacturing and non-active part costs. AF-PMSG has the highest cost due to PMs needed for the double-rotor topology, but is easier to manufacture and more lightweight compared to the other two PMSGs. The RFOR- and RFIR-PMSGs have lower estimated cost of active materials compared to that for AF-PMSG.

In order to estimate the total cost of the small-scale PMSG an estimated manufacturing cost factor (K) is introduced. It is thus considered that for AF-PMSG, $K = 1.5$, meaning that the manufacturing cost is 50% of the cost of active materials, while for RFOR- and RFIR-PMSGs, $K = 2$, due to more complex manufacturing processes.

The lowest total estimated costs result for the three-phase small-scale AF-PMSG.

Table I: Comparative main design results of the three-phase small-scale PMSGs under study

	AF-PMSG	RFOR-PMSG	RFIR-PMSG
Copper weight	11.64 kg	8.3 kg	9.14 kg
Permanent-magnet weight	10.06 kg	7.5 kg	5.55 kg
Iron weight	18.14 kg	32.8 kg	44.69 kg
Shaft weight	-	22.3 kg	5.41 kg
Total weight	39.84 kg	70.9 kg	59.39 kg
Efficiency	92 %	89.23 %	92.32 %
Turns per phase	2000	234	282
Turns per coil	500	39	47
Wire diameter	0.56 mm^2	1.4 mm^2	1.4 mm^2
Phase resistance	12 Ohm	3.4 Ohm	2.54 Ohm
Airgap	1 mm	0.8 mm	1 mm
Number of poles (PM - rotor)	16	30	30
Outer radius	295 mm	250 mm	140 mm
Stack length	-	300 mm	200 mm
Active materials estimated cost	**609.8 Euro**	**535.65 Euro**	**478.12 Euro**
Manufacturing cost factor (K)	**1.5**	**2**	**2**
Total estimated costs	**914.7 Euro**	**1071.3 Euro**	**956.24 Euro**

Conclusion

Three topologies of small-scale PMSGs have been considered for micro-wind turbine application, and comparatively studied through preliminary design and FE field analysis. The main design results have shown that AF-PMSG and RFIR-PMSG topologies have similar efficiencies, slightly higher than that of RFOR-PMSG. Although AF-PMSG has the most costly active materials, its overall estimated costs are lower compared with those of RFOR- and RFIR-PMSG topologies, mainly due to its cheaper manufacturing costs.

Acknowledgement

This work was supported by Romanian Executive Unit for Financing Higher Education, Research, Development and Innovation (UEFISCDI) from the research project with the code PN-II-PT-PCCA-2011-3.2-1696.

References

[1] B.J. Chalmers, W.Wu and E. Spooner, “An axial-flux permanent-magnet generator for a gearless wind energy system”, *IEEE Trans. Energy Convers.,* Vol. 14, No. 2, pp. 251-257, 1999.
[2] J.F. Gieras, R.-J. Wang, M.J. Kamper, *Axial flux permanent magnet brushless machines*, 2nd edition, Springer-Verlag, 2008
[3] A. Parviainen, *Design of axial-flux permanent magnet low-speed machines and performance comparison between radial-flux and axial-flux machines*, Ph.D. Thesis, Lappeenranta Univ. of Technology, Finland, 2005.
[4] J.R. Bumby and R. Martin, ”Axial-flux permanent-magnet air-cored generator for small-scale wind turbines”, *Proc. IEE – Electr. Power Applic.*, Vol. 152, No. 5, pp 1065-1075, 2005.
[5] A.A. Pop, F. Gillon and M.M. Radulescu, “Modelling and permanent-magnet shape optimization of an axial-flux machine”, *Proc. Int. Conf. Electr. Mach. – ICEM 2012*, pp. 357-363, 2012.
[6] A. Mahmoudi, H.W. Ping and N.A. Rahim, "A comparison between the TORUS and AFIR axial-flux PM machine using finite element analysis”, *Proc. IEEE Int. Electr. Mach. Drives Conf. – IEMDC 2011*, pp. 242-247.
[7] A. Di Gerlando *et al.*, Axial-flux PM machines with concentrated armature windings: design analysis and test validation of wind energy generators, *IEEE Trans. Ind. Electron.*, Vol. 58, No. 9, pp. 3795-3805, 2011.
[8] Y. Chen, P. Pillay and A. Khan, “PM wind generator topologies”, *IEEE Trans. Ind. Applicat.*, Vol. 41, No. 6, pp. 1619–1626, 2005.
[9] http://www.jmag-international.com/
[10] F. Wang *et al.*, “Design features of low-speed permanent-magnet generator direct driven by wind turbine”, *Proc. 8th Int. Conf. Electr. Mach. Syst. – ICEMS 2005*, pp. 1017-1020, 2005.
[11] J. Chen, V.N. Chemmangot and L. Xu. “Design and finite element analysis of an outer–rotor permanent–magnet generator for directly coupled wind turbines”, *IEEE Trans. Magn.*, Vol. 36, No. 5, pp. 3802–3809, 2000.
[12] http://www.speed-emachine-design.com/